Time-resolved Spectroscopy and Charge-transfer Photochemistry of Aromatic EDA Complexes with X-Pyridinium Cations

T. M. Bockman, K. Y. Lee and J. K. Kochi *
Department of Chemistry, University of Houston, Houston, Texas 77204-5641, USA

Direct photoexcitation of 1:1 aromatic EDA complexes with various *N*-substituted X-pyridinium cations (X = nitro, fluoro, methoxy and acetoxy) is achieved by the specific irradiation of their charge-transfer (CT) absorption bands. Time-resolved picosecond spectroscopy refers to charge-transfer activation by the identification of the aromatic cation radical as the initial transient (T_1) formed in a photoinduced electron-transfer together with the X-pyridinyl radical. The homolytic fragmentation of the latter varies with the X-substituent in the order X = NO_2 > F > AcO > CH_3O, and the addition of X$^{\bullet}$ to the aromatic donors leads to a series of cyclohexadienyl adducts that are identified as longer-lived transients (T_2) by time-resolved (nanosecond/microsecond) spectroscopy. The phototransients T_1 and T_2 together account for the different types of aromatic product (resulting from ring substitution, side-chain substitution and dimerization) that are generated by steady-state CT photochemistry of the aromatic EDA complexes with X-pyridinium cations.

Electrophilic aromatic substitution can be efficiently carried out with various X-pyridinium salts such as those from X = NO_2 (nitration),[1] F (fluorination),[2] NO (nitrosation),[3] *etc.* In the

$$ArH + X\text{–}Py^+ \longrightarrow ArX + H\text{–}Py^+ \quad (1)$$

case of *N*-nitropyridinium cations, we recently showed that electrophilic aromatic nitration proceeds *via* a multistep pathway involving the pre-equilibrium formation of an electron donor–acceptor (EDA) complex,[4,5] Scheme 1.

$$ArH + O_2NPy^+ \overset{K_{EDA}}{\rightleftharpoons} [ArH, O_2NPy^+] \quad (2)$$

$$[ArH, O_2NPy^+] \xrightarrow{slow} ArNO_2 + HPy^+ \quad (3)$$

Scheme 1

In a more general context, the formation of the aromatic EDA complex with the *N*-nitropyridinium electrophile in eqn. (2) mirrors that observed with a variety of other readily available X-pyridinium cations, including those with X = fluoro, acetoxy, methoxy and methyl, as described in the foregoing study.[6] Particularly diagnostic of such complexes is the appearance in the electronic spectra of new absorption bands that vary monotonically with the ionization potential and the reduction potential of ArH and X–Py$^+$, respectively. Since these spectral shifts are characteristic of charge-transfer excitation of the EDA complex according to Mulliken theory,[7,8] eqn. (4), we employ

$$[ArH, X\text{–}Py^+] \xrightarrow{h\nu_{CT}} [ArH^{+\bullet}, X\text{–}Py^{\bullet}] \quad (4)$$

(picosecond) laser-flash techniques in this study, to probe directly the charge-transfer excited state in eqn. (4), especially as it is affected by the variation of the heteroatom substituent X. From a mechanistic perspective, such a *photo-induced* electron transfer within the aromatic EDA complex could bear directly on the activation process for the *thermal* (adiabatic) substitution in Scheme 1 [as included in eqn. (3)].[9,10] Accordingly, the temporal evolution of the radical ion pair in eqn. (4) is followed into the nanosecond and microsecond (time) domains, and the reactive intermediates traced to their ultimate fate by the identification of the aromatic products.

Results

Charge-transfer Spectra of Aromatic EDA Complexes with X-Pyridinium Cations.—In order to ensure the specific irradiation of only the charge-transfer or CT band of the EDA complexes (and not the local bands of the uncomplexed arene or X-pyridinium), the absorption spectra of the various donor/acceptor combinations examined in this study were carefully monitored. Table 1 lists the low-energy cut-offs (nm) of selected aromatic donors and X-pyridinium acceptors at which their absorbances were unmeasurable (*i.e.*, A_{Ar} or A_{XPy^+} < 0.05). The charge-transfer absorption bands are indicated in Table 1 as λ_{CT} (column 7) when a clearly resolved spectral maximum was delineated. The alternative measure of λ_{CT} when the maximum of the charge-transfer band could not be clearly resolved[6] is given in Table 1 (column 6) as $\lambda_{0.2}$ at which A_{CT} = 0.20.[11]

Time-resolved (Picosecond) Spectroscopy of Aromatic Charge-transfer Complexes with X-Pyridinium Cations.—To identify the reactive intermediates in the charge-transfer excitation of the aromatic EDA complexes with X-pyridinium, we initially examined the time-resolved spectra of the transients following the application of a 30 ps (fwhm) laser pulse. The third harmonic at 355 nm of the mode-locked Nd^{3+}:YAG laser was generally used to excite the charge-transfer band since the spectral data in Table 1 clearly indicated that λ_{exc} = 355 nm would not lead to the adventitious excitation of the local bands[12] of either the free (uncomplexed) aromatic donor or X-pyridinium acceptor.

Upon irradiation of the EDA complex from 4-bromoanisole (BA) and the *N*-nitropyridinium acceptor in Table 1 (entry 13) at 355 nm, an intense, broad absorption band was observed immediately. Thus Fig. 1 shows the growth of the new absorption within the bandwidth (30 ps, fwhm) of the laser pulse. [Note the segmental shifts in the spectral envelope at t < 50 ps were an instrumental artifact caused by temporal dispersion (chirp) associated with the group velocities of the various probing wavelengths.[13]] The position (λ_{max} = 510 nm) and band shape (fwhm) of the new transient at t = 50 ps coincided with the absorption spectrum of the cation radical of 4-bromoanisole (BA$^{+\bullet}$) generated previously.[14] Moreover, the same spectrum was produced by the photoinduced electron transfer from 4-bromoanisole *via* the triplet sensitization and quenching of benzophenone,[15] as described in the Experi-

Table 1 Charge-transfer absorbances of aromatic EDA complexes with X-pyridinium cations[a]

Aromatic donor		X–Py$^+$ acceptor				
(c/mol dm^{-3})	Cut-off[b]		c/mol dm^{-3}	Cut-off[c]	$\lambda_{0.2}$/nm[d]	λ_{CT}/nm
Mesitylene						
(0.24)	310	MeO–Py(CN)$^+$	0.06	330	405	
		O_2N–Py(OMe)$^+$	0.03	350	430	
		AcO–Py(CN)$^+$	0.03	340	400	
		Me–Py(CN)$_2^+$	0.02	320	410	
Hexamethylbenzene						
(0.40)	310	F–Py$^+$	0.02	345	370	
		MeO–Py$^+$	0.02	330	355	
		O_2N–Py(OMe)$^+$	0.02	350	365	
		AcO–Py$^+$	0.02	340	380	
4-Bromoanisole						
(0.40)	312	MeO–Py$^+$	0.06	330	335	
		AcO–Py$^+$	0.10	340	360	
		F–Py$^+$	0.06	345	360	
		MeO–Py(CN)$^+$	0.06	330	415	
		O_2N–Py(OMe)$^+$	0.03	350	415	
4-Chloroanisole						
(0.40)	310	MeO–Py$^+$	0.11	330	340	
Naphthalene						
(0.08)	350	F–Py(Cl_2)$^+$	0.03	350	420	380
1,4-Dimethylnaphthalene						
(0.10)	360	AcO–Py$^+$	0.02	340	380	
9-Methylanthracene						
(0.06)	420	O_2N–Py(OMe)$^+$	0.05	350	560	466
		Me–Py(CN)$_2^+$	0.03	320	670	

[a] In acetonitrile solutions of aromatic donor with various X–Py$^+$ (concentrations indicated) at 23 °C. [b] Low-energy cut-off in nm (A < 0.05) of arene alone. [c] Low-energy cut-off (nm) of X–Py$^+$ alone. [d] Wavelength at which A_{CT} = 0.2 of the unresolved charge-transfer band (see ref. 11).

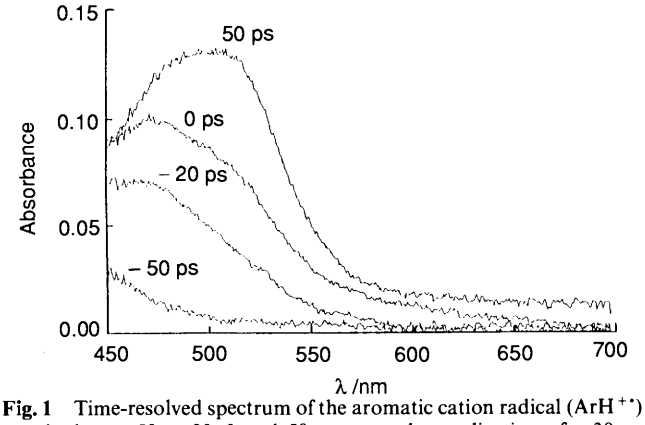

Fig. 1 Time-resolved spectrum of the aromatic cation radical (ArH$^{+\bullet}$) acquired at −50, −20, 0 and 50 ps upon the application of a 30 ps (fwhm) laser pulse at 355 nm to an acetonitrile solution of 0.4 mol dm^{-3} 4-bromoanisole and 0.03 mol dm^{-3} *N*-nitro-4-methoxypyridinium at 23 °C

mental section. Bromoanisole cation radical was also observed spectrally in the CT excitation of the analogous EDA complex with the *N*-methoxypyridinium acceptor (Table 1, entry 12), but with the diminished (absorbance) intensity listed in Table 2.

The charge-transfer excitation of the EDA complex of mesitylene and the X-pyridinium acceptors with X = NO_2, OCH_3 and OAc led to the same transient absorption as that produced from *N*-methylpyridinium. The characteristic spectrum with λ_{max} = 465 nm was identical with that of the mesitylene cation radical (MES$^{+\bullet}$) produced from pulse radiolysis.[16] The spectral intensity of the mesitylene cation radical generated (at t = 0 ps) from the various X-pyridinium complexes decreased with the electronegativity of X in the order: NO_2 > OCH_3 > OAc > CH_3 (see column 8, Table 2).

The EDA complexes of 9-methylanthracene (MA) with the *N*-nitro and *N*-methylpyridinium acceptors in Table 2 immediately gave rise to the characteristic spectrum of 9-methylanthracene cation radical (MA$^{+\bullet}$, λ_{max} = 690 nm) when it was irradiated with the 30 ps laser pulse at λ_{exc} = 532 nm (corresponding to the second harmonic of the Nd^{3+}:YAG laser). This absorption spectrum was the same as that of MA$^{+\bullet}$ previously generated by the CT excitation of the analogous complex with tetranitromethane,[17] or by the quenching of the methylanthracene triplet with methylviologen.[15]

Aromatic cation radicals were consistently observed in the earliest (picosecond) phases of the photo-activation of all the aromatic EDA complexes with X-pyridinium acceptors, as described above. The charge-transfer formulation in eqn. (4) requires the co-production of X-pyridinyl radicals that are expected to absorb in the region (350 < λ_{max} < 400 nm) with ε_{max} ~ 5000 dm^3 mol^{-1} cm^{-1}, as judged by the absorption spectra of stable *N*-alkylpyridinyl radicals.[18] Unfortunately, the spectral window of the picosecond laser system limited our temporal observations to the somewhat restricted (visible) region between 450 and 800 nm.[19]

Spectral Evolution of Short-lived Aromatic Cation Radicals in Solution.—The temporal evolution of the aromatic cation radicals (ArH$^{+\bullet}$) attendant upon the CT excitation of the various aromatic EDA complexes was found to be largely dependent on the *N*-substituent of the X-pyridinium acceptor. For convenience, the temporal behaviour of the spectral transient can be classified into three categories, which are described as follows.

Table 2 Time-resolved (picosecond) spectroscopy of aromatic EDA complexes with X-pyridinium cations[a]

Aromatic donor		$X\overset{+}{N}C_5H_xY$ Acceptor				$ArH^{+\bullet}$[c]		
	c/mol dm^{-3}	X	Y	c/mol dm^{-3}	A_{CT}[b]	λ_{max}	A_{max}	R[d]
BA	0.22	O_2N	4-OCH_3	0.03	0.80	510	0.13	1.0
	0.35	CH_3O	4-CN	0.06	0.80	510	0.02	0.3
	0.24	F	3,5-Cl_2	0.03	0.78	510	0.12	0.9
	0.40	AcO	4-CN	0.02	0.81	510	0.04	0.5
MES	0.24	O_2N	4-OCH_3	0.03	0.85	465	0.06	0.6
	0.24	CH_3O	4-CN	0.06	1.6	465	0.02	0
	0.24	AcO	4-CN	0.03	0.95	465	0.01	0
	0.24	CH_3	3,4-$(CN)_2$	0.02	1.2	465	0.01	0
MA[e]	0.06	O_2N	4-OCH_3	0.05	0.53	690	0.22	1.0
	0.05	CH_3	3,4-$(CN)_2$	0.03	0.67	690	0.01	0

[a] Following the 30 ps (fwhm) laser pulse in acetonitrile solution with λ_{exc} = 355 nm, unless indicated otherwise. BA = 4-bromoanisole, MES = mesitylene, MA = 9-methylanthracene. [b] CT absorbance at λ_{exc}. [c] Transient aromatic cation radical with spectral maximum (nm). [d] Residual absorbance (at 300 ps)/maximum absorbance (see the text). [e] λ_{exc} = 532 nm.

(*a*) Type I behaviour was exemplified by the spectral evolution of aromatic cation radicals derived from bromoanisole and methylanthracene with the *N*-nitropyridinium acceptor in Table 2. Thus Fig. 2(*a*) shows the absorption band of $BA^{+\bullet}$ (monitored at λ_{mon} = 510 nm) to rise monotonically from the (zero) baseline within the time (30 ps) of the laser pulse, and then persist unchanged in shape and intensity throughout the monitoring period (from < 50 ps out to 5 ns).

(*b*) Type II behaviour was observed with (*i*) the mesitylene cation radical produced from either the *N*-methoxy-, *N*-acetoxy- or *N*-methylpyridinium acceptors in Table 2 and (*ii*) the methylanthracene cation radical from the *N*-methylpyridinium complex. Fig. 2(*b*) shows the typical rise of the $ArH^{+\bullet}$ absorbance to a (severely limited) maximum that was followed by a very rapid decrease back to the baseline within 100 ps.

(*c*) Type III behaviour shown in Fig. 2(*c*) represents a composite between Types I and II in that the usual rise of the $ArH^{+\bullet}$ absorbance (to an intermediate value) was followed by a rapid decay to a residual absorbance (A_{res} > 0) which underwent no further change out to 5 ns. This kinetic behaviour was evident with the aromatic cation radicals produced during the CT excitation of the donor–acceptor combinations mesitylene/nitropyridinium and bromoanisole/methoxypyridinium, as listed in Table 2 (entries 5 and 2).

More generally, the residual absorbance of $ArH^{+\bullet}$ can be expressed in a normalized form, *i.e.*, $R = A_{res}/A_{max}$, where A_{max} is the maximum absorbance observed during the spectral evolution of the aromatic cation radical. Thus the limits of R for Types I and II are 1.0 and 0, respectively; and 1.0 > R > 0 for Type III behaviour. The dramatic effect of the X-pyridinium acceptor on the residual absorbance of $ArH^{+\bullet}$ is illustrated in Fig. 3 (for the methylanthracene cation radical) by the precipitous drop of R = 1.0 to 0 merely upon the change of X = nitro to X = methyl. Table 2 lists the values of R (column 9) observed with the various combinations of ArH and $X\text{–}Py^+$ in acetonitrile solutions at 23 °C.

Time-resolved (Nanosecond) Spectroscopic Studies of Long-lived Transients.—In order to follow the spectral decays into the longer time domains (especially for those showing Type I and III behaviour with $R \neq 0$), the charge-transfer excitations were carried out with a second spectrometric unit that consisted of a Q-switched Nd^{3+}:YAG laser with 10 ns (fwhm) resolution for spectral observations extending down into the microsecond region. It is also important to emphasize that the significantly wider spectral window allowed in the ns/μs measurements (see the Experimental section) enabled the absorption spectra of the CT transients to be examined between 300 < λ < 1050 nm.

For the time-resolved nanosecond studies, the EDA complexes with various X-pyridinium acceptors were initially investigated with 4-bromoanisole as the common donor in order to exploit the strong absorption band of the cation radical ($BA^{+\bullet}$, ε_{max} = 8200 dm^3 mol^{-1} cm^{-1}). Thus the irradiation of the bromoanisole complex with the *N*-acetoxypyridinium acceptor (using the 10 ns laser pulse from the third harmonic at 355 nm) gave rise to the absorption spectrum (Fig. 4) consisting of a composite of two transients T_1 and T_2. The first transient T_1 with λ_{max} = 510 nm was clearly associated with bromoanisole cation radical (*vide supra*). Fig. 4 also shows the complete (absorbance) decay of T_1 to occur to the baseline in less than 100 μs, while the second transient T_2 (λ_{max} = 420 nm) remained relatively undiminished. The inset to Fig. 4 follows the subsequent, slow decay of T_2 to the baseline over the longer time interval extending beyond 400 μs. Charge-transfer excitations of the bromoanisole complexes of the X-pyridinium acceptors with X = methoxy and fluoro afforded similar composite spectra consisting of the characteristic absorption band of $BA^{+\bullet}$, together with that of the second transient T_2. The latter were generally obscured by the high energy-tail of the strong λ_{max} = 510 nm band, and revealed themselves in Fig. 4 only as $BA^{+\bullet}$ decayed to the baseline. The spectral shift of λ_{max} for transient T_2 occurred in the order: X = OMe > OAc > F as listed in Table 3, entries 4–6.

The temporal behaviour of the transient T_2 was investigated with the X-pyridinium complexes of hexamethylbenzene, since the spectral characteristics of the cation radical ($HMB^{+\bullet}$, λ_{max} = 495 nm, ε_{max} = 2000 dm^3 mol^{-1} cm^{-1}) were less likely (than $BA^{+\bullet}$) to obscure the absorption bands of T_2 at early times. Indeed, the CT excitation of the hexamethylbenzene complex with the *N*-acetoxypyridinium acceptor at 355 nm led at early times to the composite spectrum in Fig. 5 arising from $HMB^{+\bullet}$ and transient T_2 with λ_{max} = 400 nm. The subsequent decay of T_2 at longer times (up to 1 ms) is shown in the inset of Fig. 5. Similarly, the *N*-methoxypyridinium acceptor afforded the transient spectra of $HMB^{+\bullet}$ and the transient T_2 with λ_{max} = 430 nm, but the (absorbance) growth of T_2 was not apparent. Contrastingly, the clean spectral resolution of $HMB^{+\bullet}$ and transient T_2 was not achieved in the CT excitation of hexamethylbenzene complex with the *N*-fluoropyridinium acceptor. Only a single broad band with λ_{max} ~440 nm that presumably encompassed both $HMB^{+\bullet}$ and T_2 was observed, and it remained unresolved as it slowly decayed to beyond 50 μs.

A variety of other transient spectra of aromatic cation radicals was also observed on the microsecond timescale following the CT excitation of different aromatic EDA complexes with X-pyridinium cations by using the 10 ns laser pulse

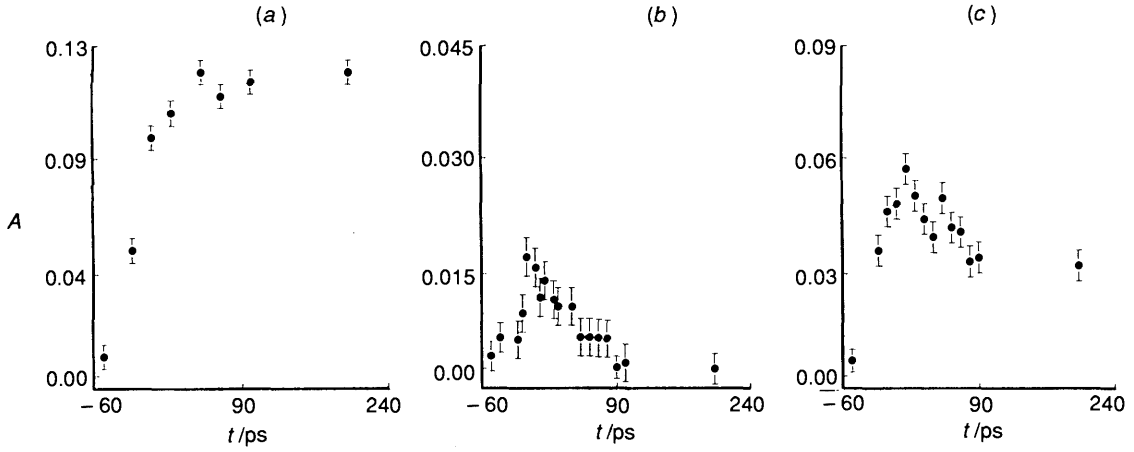

Fig. 2 Temporal evolution of $ArH^{+\bullet}$ showing typical (*a*) Type I, (*b*) Type II and (*c*) Type III behaviour from the CT excitation of bromoanisole/*N*-nitro-4-methoxypyridinium, mesitylene/*N*-methoxy-4-cyanopyridinium, and mesitylene/*N*-nitro-4-methoxypyridinium EDA complexes, respectively

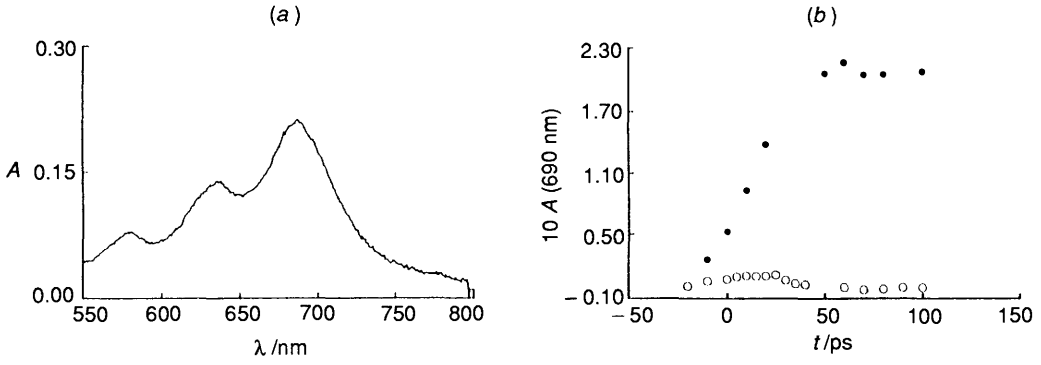

Fig. 3 (*a*) Transient absorption spectrum of the methylanthracene cation radical ($MA^{+\bullet}$) acquired at 80 ps following the 532 nm excitation of 0.06 mol dm^{-3} 9-methylanthracene and 0.05 mol dm^{-3} *N*-nitro-4-methoxypyridinium in acetonitrile at 23 °C; (*b*) effect of the electron acceptor on the temporal evolution of $MA^{+\bullet}$ as measured at λ_{mon} = 690 nm from (*a*) above (upper curve) and from the corresponding EDA complex with *N*-methyl-3,4-dicyanopyridinium (lower curve) to illustrate Type I and II behaviour, respectively

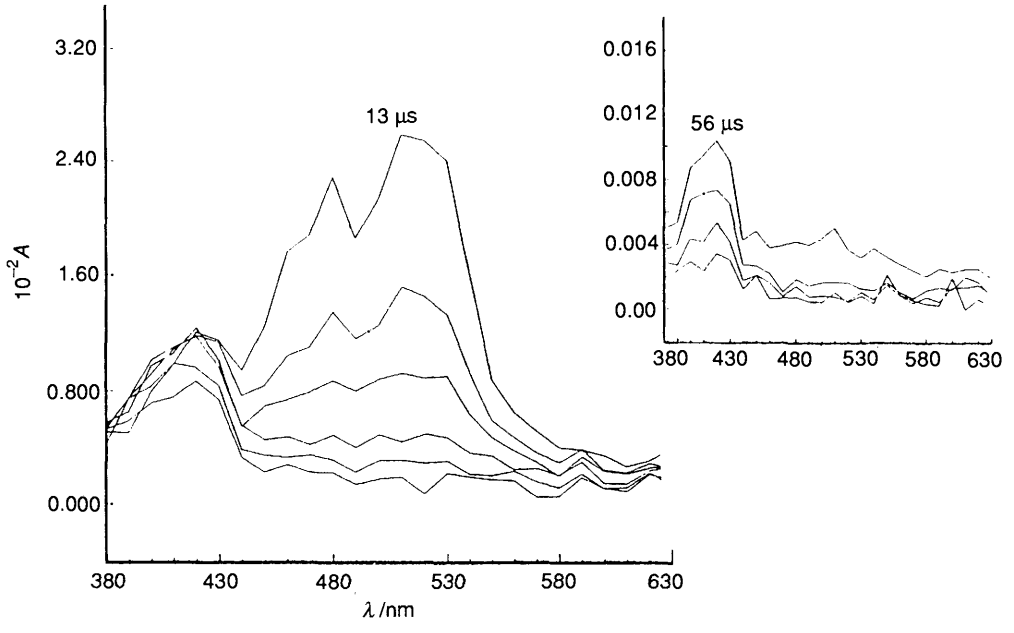

Fig. 4 Overlapping (transient) spectra of $BA^{+\bullet}$ (T_1) with λ_{max} = 500 nm and the spectral transient T_2 with λ_{max} = 420 nm acquired at 13, 18, 22, 32, 41 and 60 μs following the 532 nm excitation of 0.4 mol dm^{-3} 4-bromoanisole and 0.06 mol dm^{-3} *N*-acetoxypyridinium in acetonitrile. Inset shows the further decay of T_2 at *t* = 56, 104, 200 and 390 μs.

at 355 nm. Thus the naphthalene and 1,4-dimethylnaphthalene complexes with the pyridinium acceptors in Table 3 produced the time-resolved spectra of the cation radicals as the π-complexes[20] with λ_{max} = 570 and 600 nm, respectively. The *N*-methoxypyridinium complex with 4-chloroanisole gave a transient that was tentatively assigned to the chloroanisole

Table 3 Long-lived transients in charge-transfer activation of aromatic EDA complexes with X-pyridinium cations[a]

Aromatic donor		X–Py$^+$ acceptor			
	c/mol dm^{-3}	X	c/mol dm^{-3}	$\lambda_{max}(T_1)$/ nm	$\lambda_{max}(T_2)$/ nm
Hexamethylbenzene	0.05	F	0.02	*b*	420
	0.06	CH_3O	0.02	495	430
	0.05	AcO	0.02	495	400
4-Bromoanisole	0.4	F	0.06	510	410
	0.4	CH_3O	0.10	520	440
	0.4	AcO	0.06	510	420
Naphthalene	0.08	F	0.03	570	440
1,4-Dimethylnaphthalene	0.50	AcO	0.02	600	410
4-Chloroanisole	0.4	CH_3O	0.11	455	420

[a] Following the 10 ns (fwhm) laser pulse in acetonitrile solutions with λ_{exc} = 355 nm at 23 °C. [b] Not resolved.

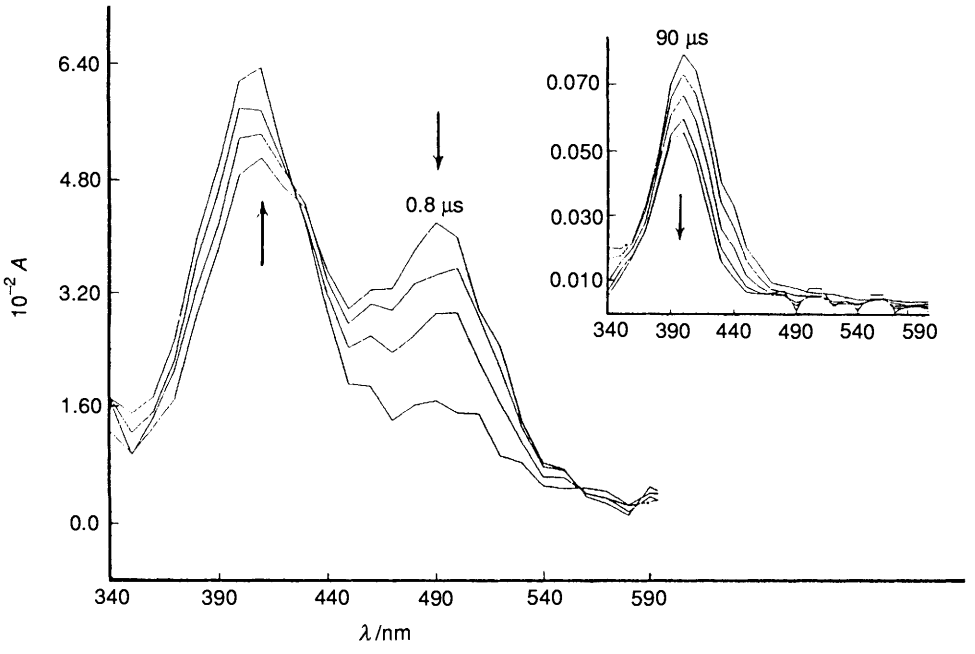

Fig. 5 Spectral decay of $HMB^{+\bullet}$ (T_1) with λ_{max} = 500 nm and the spectral growth of the transient T_2 with λ_{max} = 400 nm acquired at 0.8, 1.8, 3.6 and 9.2 μs following the 355 nm excitation of 0.05 mol dm^{-3} hexamethylbenzene and 0.02 mol dm^{-3} *N*-acetoxypyridinium in acetonitrile. The inset shows the partial decay of T_2 at t = 90, 140, 220, 440 and 880 μs.

cation radical with λ_{max} = 450 nm.[14] In each case, the absorption spectrum of the aromatic cation radical was accompanied by an additional transient spectrum (T_2 showing a weak band in the 400–450 nm region) which persisted after the spectral decay of the aromatic cation radical to the baseline in the timespan 50–100 μs.

Charge-transfer Photochemistry of Aromatic EDA Complexes with X-Pyridinium Acceptors.—The spectral transients revealed by the foregoing time-resolved (ps and ns/μs) spectroscopic studies were reconciled with the charge-transfer activation of the [ArH, X–Py$^+$] complexes by an accompanying chemical analysis of the distinctive products formed upon *steady-state* photolysis. The photochemical studies were carried out in acetonitrile with a mixture of the aromatic donors and X-pyridinium acceptors (listed in Table 4) by the continuous radiation from a 500 W mercury lamp over the course of several hours. The specific use of sharp cut-off filters with the actinic output (*e.g.*, λ_{exc} > 350 nm) ensured the excitation of only the charge-transfer absorption band of the EDA complex; and there was no ambiguity arising from the adventitious local excitation[21] of the uncomplexed reactants under these conditions. The photochemical transformations were continuously monitored by UV–VIS spectrophotometry until no further spectral change occurred. Aqueous work-up of the photolysate followed by product analysis (see the Experimental section for details) indicated that the aromatic donors generally underwent three types of chemical transformations. For example, the steady-state photolysis of the durene EDA complex with *N*-fluoropyridinium yielded a mixture of two fluorinated durenes and the aromatic dimer[22a] in Scheme 2.

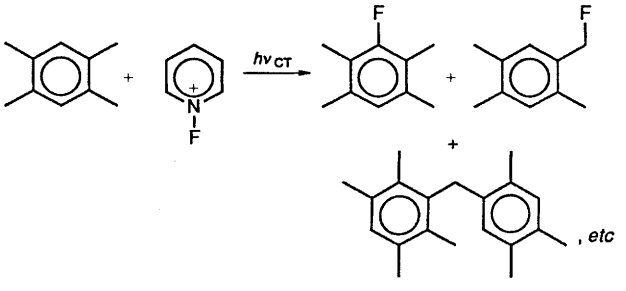

Scheme 2

Pentamethylbenzene was analogously converted into a mixture of fluoropentamethylbenzene, tetramethylbenzyl fluoride

Table 4 Charge-transfer photochemistry of aromatic EDA complexes with X-pyridinium cations[a]

ArH	XNC_5H_xY acceptor X	Y	Cut-off[b] (nm)	T/°C	t/h[c]	Product/μmol R	SC	D	Material bal. (%)[d]
DUR	O_2N[e]	4-OMe	415	23	16[f]	3.0	35	1.0	87
	F	H	300	23	8	0.8	0.8	4.3	43
	F	3,5-Cl_2	350	0	7	0.5	0.5	17.5	93
	AcO	4-CN	340	23	8	*g*	*g*	*g*	100[h]
PMB	O_2N[i]	H	400	−40	5[f]	2	14	11	99
	F	H	300	23	8	3	—	9	73
	F	3,5-Cl_2	350	0	7	1	1	5.7	66
	AcO	4-CN	340	23	8	3[j]	—	1	67
HMB	O_2N[k]	4-OMe	400	23	10[f]	—	59[l]	—	100 (85)[m]
	F	3,5-Cl_2	350	23	8	—	1[n]	—	72
NAPH	O_2N[o]	4-OMe	380	23	5[f]	15	—	—	78
	F	3,5-Cl_2	380	0	3	21	—	—	72 (83)[m,x]
	AcO	4-CN	380	23	12	*g*	*g*	*g*	82[p]
	CH_3O	4-CN	380	23	12	*g*	*g*	*g*	70[w]
DMN	F	3,5-Cl_2	415	0	3	33[q]	—	—	75
	F	3,5-Cl_2	—	23	48[r]	55[q]	—	—	92 (87)[m]
	AcO	4-CN	410	23	10	4[j]	—	—	70
	CH_3O	4-CN	410	23	10	5	—	—	83
MN	F	3,5-Cl_2	380	0	4	27[s]	—	6	95 (87)[m]
ANTH	F	3,5-Cl_2	425	0	8	20[t]	—	—	72
	AcO	4-CN	425	23	8	3[j]	—	—	65
	CH_3O	4-CN	410	23	10	1	—	—	62
MA	F	3,5-Cl_2	480	0	1	13	—	20[u]	98 (68)[m]
	F	3,5-Cl_2	—	23	12[r]	14	—	15[u]	82
	AcO	4-CN	460	23	15	—	—	6	100[v]
	CH_3O	4-CN	460	23	40	25	—	3[u]	80 (92)[m]

[a] In acetonitrile (2 cm^3) containing 60 μmol each of $X\text{–}Py^+$ and ArH, unless indicated otherwise. DUR = durene, PMB = pentamethylbenzene, HMB = hexamethylbenzene, NAPH = naphthalene, DMN = 2,6-dimethoxynaphthalene, MN = 1-methoxynaphthalene, ANTH = anthracene, MA = 9-methylanthracene. [b] Sharp cut-off filter (see the Experimental section). [c] Of irradiation. [d] Based on recovered ArH. [e] From 130 μmol DUR and 70 μmol $O_2N\text{–Py(OMe)}^+$. [f] See ref. 24. [g] Less than 0.1 μmol. [h] 40% $AcO\text{–Py(CN)}^+$ decomposed. [i] From 160 μmol PMB and 260 μmol $O_2N\text{–Py(OMe)}^+$. [j] Mixture of acetoxy and methyl derivatives. [k] From 110 μmol HMB and 110 μmol $O_2NPy(OMe)^+$. [l] Mixture of nitro and nitrito. [m] Based on hydropyridinium ($H\text{–Py}^+$). [n] Acetamido. [o] From 50 μmol NAPH and 100 μmol $O_2N\text{–Py(OMe)}^+$. [p] $AcO\text{–Py(CN)}^+$ completely consumed and 49 μmol NAPH recovered. [q] Single isomer and difluoro derivative(s). [r] In the dark. [s] Mixture of isomers. [t] Includes difluoro derivative(s). [u] Includes unidentified biaryls. [v] 60% $AcO\text{–Py(CN)}^+$ decomposed. [w] $MeO\text{–Py(CN)}^+$ completely decomposed. [x] 2 μmol $F\text{–Py(3,5-Cl}_2)^+$ recovered.

and nonamethyldiphenylmethane;[22b] but *N*-pentamethylbenzylacetamide[23] was detected as the sole product from hexamethylbenzene.

For convenience, the various aromatic products are designated generically in Table 4 as R, SC and D to represent *ring* substitution, *side-chain* substitution and aromatic *dimerization*, respectively. Since they were produced only upon the specific irradiation of the aromatic EDA complexes with X-pyridinium acceptors, the photochemical process is hereafter referred to as *charge-transfer substitution* (*dimerization*). For comparative purposes, Table 4 also includes the charge-transfer nitration of some selected aromatic donors with the *N*-nitropyridinium acceptors from a separate study.[24]

Ring fluorination was the primary process in the charge-transfer activation of the *N*-fluoropyridinium EDA complexes with the polycyclic naphthalene and anthracene donors, as well as their (methyl and methoxy) analogues. In each case, the (liberated) aromatic proton was identified as a mixture of the hydropyridinium cation and hydrogen fluoride,[25] Scheme 3.

The charge-transfer fluorination of 1-methoxynaphthalene yielded three isomeric fluoro-1-methoxynaphthalenes in addition to a small amount of difluorinated products (by GC–MS and ^{19}F NMR analysis), together with the 1-methoxynaphthalene dimer(s).[26] Anthracene gave 9-fluoroanthracene (45%) as the major product together with small amounts (6%) of difluoroanthracene. Under similar reaction conditions, the

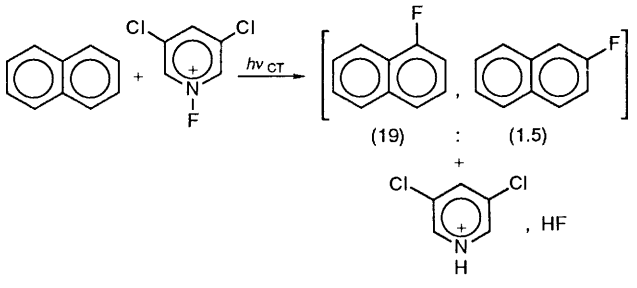

Scheme 3

photoactivation of the analogous 9-methylanthracene EDA complex afforded more or less equimolar amounts of the ring-fluorinated anthracene[27] and the unique dimer lepidopterene,[28] Scheme 4, together with small amounts of an unidentified (non-fluorinated) product, tentatively assigned to a biaryl structure (see the Experimental section). This photochemical transformation was carried out at 0 °C (Table 4, entry 23) to obviate competition from the slow thermal process (entry 24).

N-Methoxypyridinium participated in a pattern of CT photochemistry which was similar to that obtained with *N*-fluoropyridinium, except the effectiveness was largely limited to the polycyclic aromatic donors. Thus anthracene underwent ring methoxylation, Scheme 5. Similarly, 9-methylanthracene was converted into 9-methoxy-10-methylanthracene,[29] together

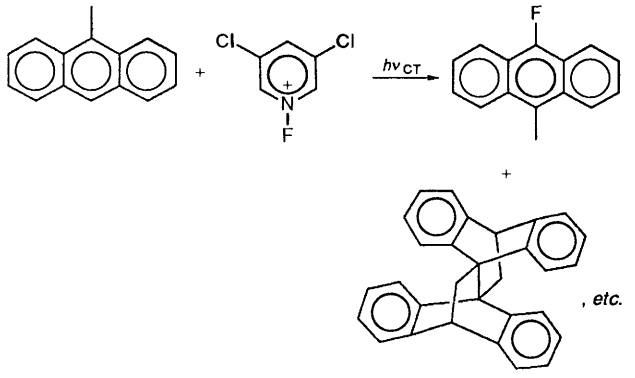

Scheme 4

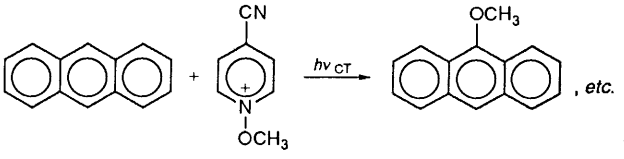

Scheme 5

with the same dimer (lepidopterene) and the unidentified (biaryl) product that was obtained with *N*-fluoropyridinium in Scheme 4. Likewise, the electron-rich 2,6-dimethoxynaphthalene was methoxylated (Table 4, entry 18), but the parent naphthalene was not (entry 14).

N-Acetoxypyridinium effected the simultaneous CT acetoxylation[30] and methylation of anthracene, Scheme 6. However,

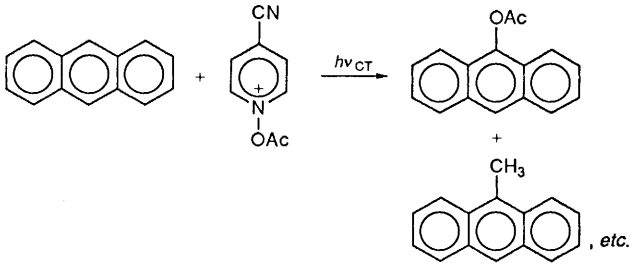

Scheme 6

9-methylanthracene under the same conditions suffered no CT substitution, the dimeric lepidopterene being the only product observed (Table 4, entry 25). Moreover, the electron-rich 2,6-dimethoxynaphthalene was both acetoxylated and methylated, but naphthalene was not. Pentamethylbenzene under the same conditions afforded both pentamethylphenyl acetate (acetoxylation) and hexamethylbenzene (methylation), as indicated in Table 4 (entry 8) under conditions in which durene was recovered unchanged.

Thermal Substitution of Aromatic Donors with X-Pyridinium Acceptors.—The coloured solutions of the aromatic donors in combination with the X-pyridinium acceptors in Table 4 remained unchanged, the CT colours being discharged only when the acetonitrile solutions were deliberately exposed to light—the exceptions being those comprising the most electrophilic X-pyridinium cations. Thus all of the *N*-methoxy- and *N*-acetoxy-pyridinium EDA complexes persisted for several days at room temperature, and only the charge-transfer bands of the *N*-fluoropyridinium complexes with the electron-rich 2,6-dimethoxynaphthalene and 9-methylanthracene bleached slowly upon standing (in the dark). For example, spectral (^{19}F and ^{1}H NMR) analysis showed the complete disappearance of the *N*-fluoropyridinium according to the stoichiometry shown in Scheme 7, the ring-fluorinated dimethoxynaphthalene being identical with that obtained by charge-transfer fluorination

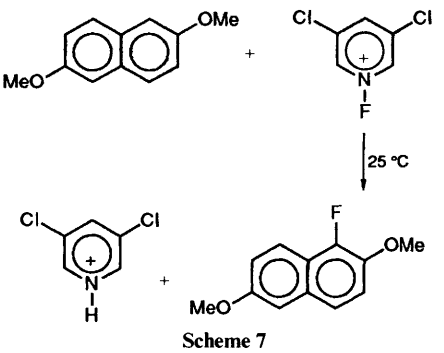

Scheme 7

(Table 4, entry 15). Moreover, all the nitropyridinium acceptors have previously been shown[5] to react thermally with the aromatic donors in Table 4 to afford the same series of ring (R) and side-chain (SC) substituted products, as well as the aromatic dimers (D).[22] At the opposite extreme of cationic reactivity, none of the *N*-methylpyridinium cations including those with 4-cyano substituents reacted with even the most electron-rich aromatic donor, either thermally or *via* charge-transfer activation.

Discussion

Time-resolved spectroscopy of the reactive intermediates (Table 2), together with the accompanying charge-transfer photochemistry (Table 4), identifies the photoexcitations of various aromatic EDA complexes with X-pyridinium acceptors according to eqn. (4). Thus Figs. 1 and 3 show the absorption spectra of typical aromatic cation radicals ($ArH^{+\bullet}$) that are formed upon the applications of the picosecond laser pulse. The characteristic spectral growth (common for all X-pyridinium acceptors) that is coincident with the characteristic risetime τ = 30 ps (fwhm) of the mode-locked Nd^{3+}:YAG laser pulse accords with the expectations of Mulliken theory of charge transfer.[7,8] However, the subsequent fate of the aromatic cation radicals is strongly dependent on the X-pyridinium acceptor, as underscored by the three typical decay patterns illustrated in Fig. 2. [Note the parallel spectral decay of the accompanying X-pyridinyl (not observed directly) is demanded by the stoichiometry in eqn. (4)].

Fast Rate Processes Associated with the Charge-transfer Activation of Aromatic EDA Complexes with X-Pyridinium Cations.—The spontaneous annihilation of the aromatic cation radical by back electron transfer (k_1) is a common pathway for the deactivation of CT-excited ion radical pairs,[31–33] eqn. (5), in

$$[ArH, X\text{-}Py^{+}] \underset{k_1}{\overset{h\nu_{CT}}{\rightleftharpoons}} [ArH^{+\bullet}, X\text{-}Py^{\bullet}] \qquad (5)$$

which the rise and fall of the transient absorbance can occur within the pulsewidth of the 30 ps (fwhm) laser. Thus, the Type II decay in Fig. 2(*b*) that is observed for the X-pyridinium acceptors with X = methyl is consistent with *N*-alkylpyridinyl radicals that are subject to facile back electron transfer with a first-order rate constant (k_1) of roughly 10^{11} s^{-1}. [Note that the rise/fall of the transient absorbance will reflect the (Gaussian) shape of the laser pulse when $k \geq 10\ \tau^{-1}$.]

The other extreme of transient behaviour is represented by the Type I pattern shown in Fig. 2(*a*), in which the aromatic cation radical undergoes no decay on the picosecond timescale—its absorbance (concentration) rising monotonically with the laser pulse to a limiting plateau. Since this transient profile is mainly observed with highly electrophilic *N*-nitropyridinium cations,[6] it cannot be ascribed to the attenuation of k_1 sufficient to preclude back electron transfer in eqn. (5). Let us therefore

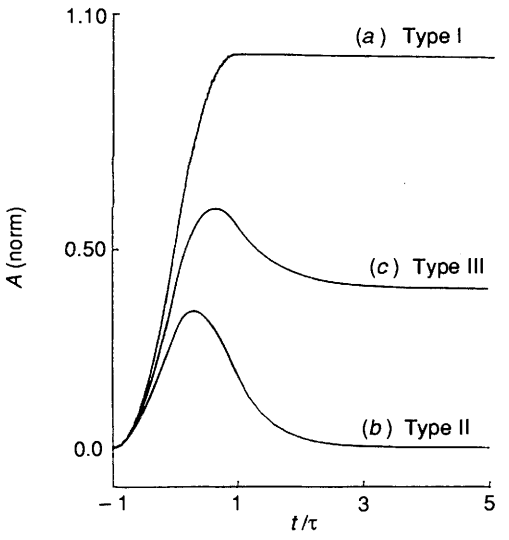

Fig. 6 Computer simulation of the absorbance change of the transient aromatic cation radical according to the mechanism in Scheme 1 for (*a*) Type I, (*b*) Type II and (*c*) Type III behaviour with $k_1 = 1/\tau$ and (*a*) $k_2 = 10/\tau$, (*b*) $k_2 = 0$ and (*c*) $k_2 = k_1$, respectively

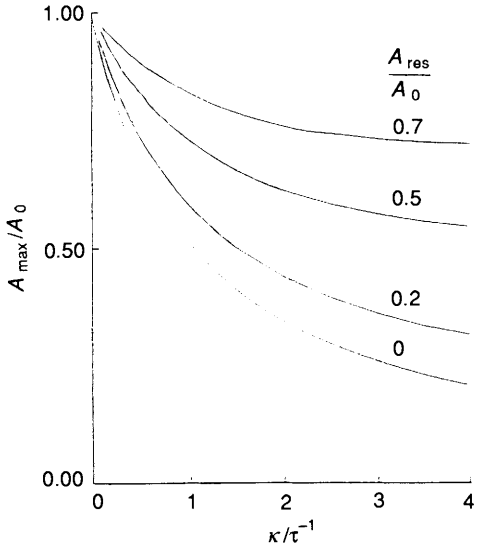

Fig. 7 Representative (theoretical) working curves for the variation of the absorbance maximum (A_{max}/A_0) with the characteristic decay constant κ at various levels of the residual absorbance (A_{res}/A_0), as indicated

consider the Type I behaviour to arise *via* an alternative pathway that diverts the aromatic cation radical from back electron transfer, namely, by the rapid decomposition (k_2) of the accompanying *N*-nitropyridinyl radical,[5] eqn. (6), that occurs

$$O_2N\text{–}Py^{\bullet} \xrightarrow{k_2} NO_2 + Py \qquad (6)$$

faster than k_1. Indeed, such a mechanistic formulation also accounts for the Type III behaviour [Fig. 2(*c*)] as an intermediate situation for Scheme 8, in which k_1 and k_2 represent *competitive* processes.

$$[ArH, X\text{–}Py^{+}] \underset{k_t}{\overset{h\nu_{CT}}{\rightleftharpoons}} [ArH^{+\bullet}, X\text{–}Py^{\bullet}] \qquad (7)$$

$$[ArH^{+\bullet}, X\text{–}Py^{\bullet}] \xrightarrow{k_2} ArH^{+\bullet} + X^{\bullet} + Py \qquad (8)$$

Scheme 8

The analytical solutions of the general kinetics for Scheme 8 (see the Experimental section) are presented as the computer simulations in Fig. 6 for various values of k_1 and k_2 relative to the laser pulsewidth (τ^{-1}). The decay profiles in Fig. 6(*a*) and 6(*b*) represent the kinetics extrema for the residual absorbance (as experimentally defined in Table 2), *i.e.*, $R = 1.0$ and 0, respectively, to describe the mechanisms in which back electron transfer is either inconsequential ($k_2/k_1 \geq 10$) or dominant ($k_2/k_1 \sim 0$). Fig. 6(*c*) describes the intermediate (kinetics) situation in which the magnitudes of k_1 and k_2 are comparable, and the 'true' residual of the transient absorbance is then given by eqn. (9) where A_{res} is the residual absorbance (measured at

$$A_{res}/A_0 = k_2/(k_1 + k_2) \qquad (9)$$

5 ns) and A_0 is the (theoretical) absorbance in the absence of kinetics [and represented in Fig. 6 by the plateau in profile (*a*)]. Although the rigorous evaluation of the individual rate constants k_1 and k_2 from eqn. (9) is not possible with the data on hand, we believe that reasonable estimates are obtainable from a comparison of the experimental profiles in Fig. 2 with the computer simulations in Fig. 6 in the following manner.

(*a*) *Type I.* The coincidence of the experimental decay [Fig. 2(*a*)] with the simulated profile [Fig. 6(*a*)] suggests that $A_{res} \sim A_0$ and $k_2 \geq 10\ k_1$ in eqn. (9). Since $k_1 \sim \tau^{-1}$, the fragmentation rate of the *N*-nitropyridinyl radical in eqn. (6) is $k_2 > 3 \times 10^{11}\ s^{-1}$, which essentially obviates back electron transfer (k_1) to re-form the EDA complex in eqn. (7).

(*b*) *Type II.* At the other extreme, the *N*-methylpyridinium acceptor consistently yields the experimental Type II decay [Fig. 2(*b*)] that coincides with simulated profile [Fig. 6(*b*)] in which the absence of a residual absorbance corresponds to $k_2 = 0$. In this kinetics situation, the rate constant k_1 can be equated to the maximum value (A_{max}) of the transient absorbance (see the Experimental section for the derivation), and the functional form of the relationship is graphically illustrated by the working curve in Fig. 7 (bottom), in which the normalized residual $A_{res}/A_0 = 0$ and the characteristic decay constant $\kappa = k_1$. The value of $k_1 = 7 \times 10^{11}\ s^{-1}$ obtained from $A_{max} = 0.05$ in Table 5 (entry 6) indicates that the *N*-methylpyridinyl radical suffers only back electron transfer. The latter also accords with the absence of productive CT photochemistry, even upon prolonged irradiation of the aromatic EDA complexes with *N*-methylpyridinium acceptors.

(*c*) *Type III.* The intermediate behaviour shown in Fig. 2(*c*) corresponds to a kinetics situation in which the relative values of k_1 and k_2 (Scheme 8) vary between the experimentally defined limits of $0.05 < (k_1/k_2) < 0.8$. As such, a set of working curves such as those in Fig. 7 can be developed (see the Experimental section) for the variation of the absorbance maximum A_{max} as a function of the characteristic decay constant κ for each level of the residual absorbance. Table 5 lists the absorbance maxima (column 4) and residuals (column 5) for various X-pyridinium acceptors after normalization relative to that (A_0) of nitropyridinium described above. The values of κ evaluated from the working curves are listed in column 6 of Table 5. The individual rate constants k_1 and k_2 in columns 7 and 8 are then computed from the combination of the values of $\kappa = k_1 + k_2$ and the residual absorbances [eqn. (9)].

Homolytic Lability of Transient X-Pyridinyl Radicals.—The rate constant k_2 in Table 5, as evaluated by the time-resolved spectroscopy of charge-transfer activation, is ascribed to the fragmentation of the X-pyridinyl radical according to Scheme 8 eqn. (8). Our inability to obtain a measurable value of k_2 for species with X = methyl, indicates that the cleavage of the N–Me bond is slow, and it generally accords with the previous isolation and characterization of stable *N*-alkylpyridinyl

Table 5 Rate constants for fragmentation and back electron transfer of CT-generated X-pyridinyl radicals[a]

Donor ArH	Acceptor X–Py$^+$	ΔG/kcal mol^{-1} [b]	A_{max}/A_0	A_{res}/A_0	$\kappa/10^{10}$ s^{-1} [c]	$k_1/10^{10}$ s^{-1}	$k_2/10^{10}$ s^{-1}
BA	O_2N–Py(OMe)$^+$	47	1.0[d]	1.0	—	$< \sim 0.3$	~ 30
BA	F–Py(Cl_2)$^+$	54	0.92	0.77	2.6	0.6	2.0
BA	AcO–Py(CN)$^+$	42	0.31	0.19	6.5	5.3	1.2
BA	MeO–Py(CN)$^+$	51	0.18	0.05	16.8	16	0.8
MA	O_2N–Py(OMe)$^+$	35	1.0	1.0	—	$< \sim 0.3$	~ 3
MA	Me–Py$(CN)_2^+$	39	0.05	0	—	70	—

[a] As in Table 2. [b] Energy gap = $E^{\circ}_{Ar} + E^{c}_{p}$ of aromatic donor and X-pyridinium acceptor, respectively, in ref. 6. [c] From Fig. 7, see the text. [d] Reference value.

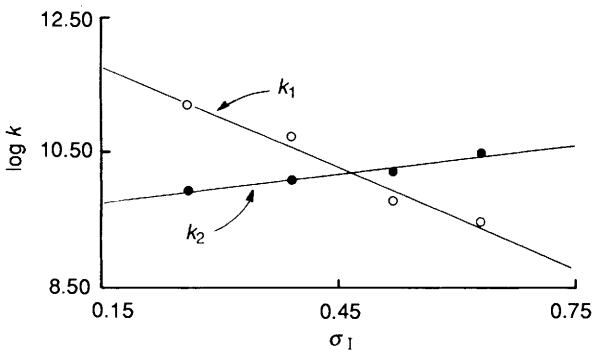

Fig. 8 Linear free energy relationships for X-pyridinyl radicals relative to their first-order fragmentation (k_2) and second-order back electron transfer with BA$^{+\bullet}$ (k_1), as evaluated by the inductive parameter σ_I

radicals.[34–37] Indeed, EPR studies of *N*-alkylpyridinyl radicals indicate that the odd (unpaired) electron is extensively delocalized in the heteroaromatic ring.[18] These neutral species are thus classified as π-radicals, being isoelectronic with the well-known aromatic anion radicals.[38] In transient alkylpyridinyl radicals, the relatively high spin density at the 2,4-positions leads to the corresponding dihydrobipyridine dimers in which the alkyl–nitrogen bonds always remain intact.[39]

By way of contrast, the measured *lower* limit of $k_2 > 3 \times 10^{11}$ s^{-1} for the *N*-nitropyridinyl radicals by time-resolved spectroscopy indicates that the homolytic cleavage of the N–NO_2 bond in eqn. (6) is extensive. This conclusion is supported by the observation of NO_2 in transient electrochemical (cathodic) studies of X–Py$^+$, including fast-scan cyclic voltammetry,[5] and by the high quantum yields of nitroaromatic compounds that are obtained from the charge-transfer activation of various aromatic EDA complexes with *N*-nitropyridinium cations.[24]

The other X-pyridinyl radicals with X = fluoro, methoxy and acetoxy are of intermediate stability, as reflected by the rate constants k_2 in Table 5 that lie between those for X = methyl and X = nitro. The dependence of the fragmentation rate constant k_2 on the X-substitution is shown in Fig. 8 by the linear free energy correlation with the (Hammett) inductive parameter σ_I.[40] The slope of $\rho_2 = 1.5$ for various X-pyridinyl radicals is consistent with the weakening of the N–X bond owing to the increased delocalization of the unpaired electron onto the antibonding orbital of the more electronegative substituents in the order: X = NO_2 > F > AcO > $CH_3O \gg CH_3$. If so, the same (or closely related) factors are also pertinent to the competition from back electron transfer as shown by the related linear free energy correlation in Fig. 8 of the rate constant k_1, but with a *reverse* slope, *i.e.*, X = CH_3O > AcO > F > NO_2. Indeed the significantly larger magnitude of $\rho_1 = -4.5$ arises from the rate of back electron transfer which rapidly increases with the increased stabilization of the X-pyridinyl radical alluded to above. The effect of odd-electron delocalization on the rate of back electron transfer can be taken in the context of Marcus theory[41] as the alteration of the inner-sphere reorganization energy (λ_i) for the redox couple: X–Py$^{\bullet}$ ⇌ X–Py$^+$. Such changes in λ_i are most likely to be manifested with substituent (σ_I) variations by varying (increased) lengths of the N–X bonds in the X-pyridinyl radicals relative to those extant in the cations.[42]

Aromatic Cation Radicals and Cyclohexadienyl Adducts as Key Intermediates in Charge-transfer Photochemistry.—Time-resolved (picosecond) spectroscopy described above identifies the aromatic cation radical (ArH$^{+\bullet}$) in the earliest phases of charge-transfer activation. The further temporal evolution of ArH$^{+\bullet}$ can be followed into the longer (ns/μs) time domains, especially when their spectral behaviour follows the Type I and III rate profiles (Fig. 2). The latter are characteristic of the facile fragmentation (k_2) of the accompanying X-pyridinyl radicals relative to back electron transfer (k_1) according to Scheme 8. Under these circumstances, a second spectral transient (T_2) can be discerned (Figs. 4 and 5), in addition to the transient (residual) spectrum of the aromatic cation radical (T_1). Most notably, the transient spectrum of T_2 with λ_{max} = 420 nm for 4-chloroanisole and MeO–Py$^+$ is akin to the absorption spectrum of the previously reported cyclohexadienyl radical of the type shown below.[43]

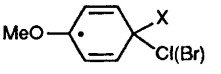

T_2

Moreover, the analogous 4-bromoanisole donor yields the family of well-resolved transient spectra (T_2 in Table 3) with λ_{max} = 410, 420 and 440 nm from the X-pyridinium acceptors with X = acetoxy, fluoro, and methoxy, respectively. Indeed, such a bathochromic shift of the absorption maxima with the variation in the X-substituent, accords with earlier observation of cyclohexadienyl radicals.[43,44]

The most direct pathway for the formation of cyclohexadienyl radicals (T_2) involves the homolytic addition of the substituent radical [*i.e.*, X$^{\bullet}$ from the fragmentation of X-pyridinyl radicals in eqn. (8)] onto the aromatic donor,[45] eqn. (10).

(10)

The formation of the cyclohexadienyl radicals in eqn. (10) is analogous to the well-studied addition of hydroxyl radicals to various aromatic substrates,[46] which occurs with rate constants in the region of 10^9 dm^3 mol^{-1} s^{-1}. Such a second-

order process can be observed in the growth of the spectral transient T_2 in Fig. 5.

The temporal behaviour of T_1 and T_2 such as is shown in Figs. 4 and 5 is not correlated—$ArH^{+\bullet}$ generally decaying faster than the concentration change of the cyclohexadienyl radicals. We thus conclude that the cross reaction of the transient pair is not a dominant pathway for the CT activation of aromatic EDA complexes from X-pyridinium acceptors with X = methoxy, fluoro and acetoxy. This kinetic situation is in strong contrast with that observed with *N*-nitropyridinium acceptors in which the liberated NO_2 is incapable of homolytic addition as described in eqn. (10).[20,24] The significant difference in the property of the *N*-nitropyridinium acceptor and the other X-pyridinium acceptors with X = methoxy, fluoro and acetoxy, insofar as their charge-transfer behaviour is concerned, can thus be ascribed to two kinetic factors. First, the rate of homolytic cleavage of *N*-nitropyridinyl radicals [$k_2 \geq 3 \times 10^{11}$ s^{-1} in eqn. (6)] is so fast that high photochemical efficiencies are achieved with minor complications from the energy-wasting back electron transfer ($k_1 < 10^{10}$ s^{-1}). Second, the cleaved fragment NO_2 is exceptionally stable (persistent),[47] to allow the cross reaction with the aromatic cation radical in eqn. (13) to be the principal fate of the reactive intermediates,[24] Scheme 9.

$$[ArH, O_2NPy^+] \xrightarrow{h\nu_{CT}} [ArH^{+\bullet}, O_2N\text{–}Py^{\bullet}] \quad (11)$$

$$[ArH^{+\bullet}, O_2N\text{–}Py^{\bullet}] \xrightarrow{\text{fast}} ArH^{+\bullet} + NO_2 + Py \quad (12)$$

$$ArH^{+\bullet} + NO_2 \xrightarrow{(-H^+)} ArNO_2 \quad (13)$$

Scheme 9

By comparison, the fragmentation rates of the X-pyridinyl radicals with X = methoxy, fluoro and acetoxy are slower than that with X = nitro, as listed in Table 5. More important however, is the significantly higher homolytic reactivity of the methoxy, fluoro and acetoxy radicals,[48] particularly towards aromatic addition and hydrogen abstraction.[49] As a result, the cross reactions with transient aromatic cation radicals [such as that in eqn. (13) for NO_2] will be relatively unimportant, and the further reactions of both reactive intermediates should follow more or less independent pathways, Scheme 10.

$$[ArH, X\text{–}Py^+] \underset{k_1}{\xrightarrow{h\nu_{CT}}} [ArH^{+\bullet}, X\text{–}Py^{\bullet}] \quad (14)$$

$$[ArH^{+\bullet}, X\text{–}Py^{\bullet}] \xrightarrow{k_2} ArH^{+\bullet} + X^{\bullet} + Py \quad (15)$$

$$ArH^{+\bullet} \xrightarrow{\text{fast}} etc. \quad (16)$$

$$X^{\bullet} \xrightarrow{\text{fast}} etc. \quad (17)$$

Scheme 10

Accordingly, let us consider how these reactive intermediates can lead to the diverse aromatic products identified in Table 4.

Chemical Fates of the Reactive Intermediates in Charge-transfer Activation of [ArH, X–Py^+] *Complexes.*—The aromatic cation radicals derived from the (poly)methylbenzene donors $Ar'CH_3$ pertinent to this study are known to be highly acidic species.[50,51] When the (poly)methylbenzene cation radicals suffer proton loss, they generate benzylic radicals[52] that are readily oxidized[53] and can lead to side-chain substitution[54] and aromatic dimers,[55] eqns. (18) and (19), where $Ar'CH_3 \equiv ArH$ and $N^- =$ nucleophiles such as X^-, $NCCH_3$, *etc.* that are present during the reaction. Likewise, the cyclohexadienyl radicals formed *via* homolytic addition in eqn. (10) are also susceptible to the rapid oxidation/deprotonation that leads to aromatic substitution,[45] *viz.* eqn. (20).

$$Ar'CH_3^{+\bullet} \xrightarrow{(-H^+)} Ar'CH_2^{\bullet} \xrightarrow{(-e^-)} \begin{cases} \xrightarrow{N^-} Ar'CH_2N & (18) \\ \xrightarrow{ArH} Ar'CH_2Ar + H^+ & (19) \end{cases}$$

$$\text{Ar}\overset{\bullet}{\underset{X}{\overset{H}{<}}} \xrightarrow{(-e^-)} H^+ + ArX \quad (20)$$

According to eqns. (18)–(20), the products of ring substitution (R) in Table 4 derive from the substituent radical ($X^{\bullet}$) *via* the cyclohexadienyl adduct, whereas the products of side-chain substitution (SC) and aromatic dimerization (D) derive principally from the aromatic cation radical ($ArH^{+\bullet}$). Consistent with this general formulation is the observed CT photochemistry of the various aromatic donors with *N*-fluoropyridinium that yields not only ring-fluorinated products but also a mixture of side-chain products including both benzylic fluorides and *N*-benzylacetamides (from $N = F^-$ or HF and $NCCH_3$). Moreover, the aromatic dimers (D) are diphenylmethane derivatives [eqn. (19)] that include lepidopterene.[28] Similarly, the CT photochemistry with *N*-methoxypyridinium affords aryl methyl ethers, and that with *N*-acetoxypyridinium leads to aryl acetates. The accompanying amounts of ring methylation observed in the latter case are readily attributed to the partial diversion of acetoxy radicals by unimolecular decarboxylation, eqn. (21), that occurs with the first-order rate constant 1.6×10^9 s^{-1}.[56]

$$CH_3CO_2^{\bullet} \xrightarrow{\text{fast}} CO_2 + CH_3^{\bullet}, etc. \quad (21)$$

Since the material balances based on the recovered ArH (Table 4, column 10) generally account for most of the aromatic donors, any unidentified aromatic product is unlikely to be formed in significant yields. However, the same conclusion does not apply to the X-pyridinium acceptor. Thus the high conversion of X–Py^+ (measured in the selected cases cited in entries 4, 13, 14 and 25) does not usually result in a corresponding amount of ring substitution (R). The latter suggests that significant amounts of $X^{\bullet}$ circumvent the addition in eqn. (10), probably by competition from hydrogen-atom transfer from the solvent (note the formation of hydrogen fluoride from F–Py^+). In this regard, the charge-transfer substitution of aromatic donors with *N*-fluoro-, *N*-acetoxy- and *N*-methoxy-pyridinium acceptors is likely to be without synthetic utility, except for the polycyclic arenes which are particularly susceptible to homolytic addition.[45]

Comments on Electrophilic Aromatic Substitutions with X-Pyridinium Cations.—X-Pyridinium cations represent a graded series of electrophilic reagents in measure with the decreasing values of their reduction potentials $E_p^c = 0.10 > -0.66 > -0.81 > -1.02 > -1.32$ V *versus* SCE for $X = NO_2 > F > AcO > CH_3O > CH_3$, respectively.[6] This property is also reflected in the relative ease with which each X-pyridinium cation effects electrophilic aromatic substitution (by thermal activation), as described in eqn. (1). Thus electrophilic aromatic nitration occurs with *N*-nitropyridinium cation attendant upon its exposure to various arene donors, including benzene derivatives.[5] In comparison, the *N*-fluoropyridinium cation effects only the aromatic fluorination of the most electron-rich polycyclic arenes, being inert to most benzene derivatives.[2] Finally, the *N*-acetoxy- and *N*-methoxy-pyridinium cations show no propensity for aromatic acetoxylation or methoxylation (except upon charge-transfer activation).

The parallel trend between the electrophilic (adiabatic) reactivity of X-pyridinium cations in eqn. (1) and the charge-transfer (non-adiabatic) transition in eqn. (4) raises the mechanistic question as to the relationship between the activated complex in the thermal process and the ion radical pair in charge-transfer photochemistry.[57] Although the low electrophilic reactivity of *N*-fluoropyridinium cations limited our comparative study to a pair of aromatic donors, the results included in Table 4 strongly point to their close relationship. For example, 9-methylanthracene reacts slowly in the dark with *N*-fluoropyridinium to produce essentially the same mixture of 9-fluoro-10-methylanthracene and the unique dimeric products that are produced by charge-transfer photochemistry (see Scheme 4 and compare entries 24 and 23 in Table 4). Similarly, the electrophilic aromatic fluorination of 2,6-dimethoxynaphthalene in the dark at room temperature yields a single fluorinated product that is identical with the fluoronaphthalene obtained by charge-transfer fluorination at 0 °C for 3 h (compare entries 16 and 15, Table 4). These comparative results mirror those recently obtained between the electrophilic nitration and charge-transfer nitration of an extensive series of aromatic donors.[24] As such they provide further insight into the generality of the charge-transfer mechanism as applied to a variety of electrophile–nucleophile interactions.[57]

Experimental

All the aromatic donors and X-pyridinium acceptors employed in this study have been described previously.[6] Acetonitrile (Fisher reagent grade) was stirred with $KMnO_4$ for 24 h and the mixture refluxed until colourless. After removal of the brown MnO_2 by filtration, the acetonitrile was distilled from P_2O_5 under an argon atmosphere. Acetonitrile was again fractionated from CaH_2 and stored in a Schlenk flask under an argon atmosphere.

Time-resolved (Picosecond) Spectroscopy of Aromatic EDA Complexes with X-Pyridinium Acceptors.—The pyridinium salts were weighed and transferred to a Schlenk flask in a Vacuum Atmospheres HE-493 drybox. Acetonitrile was added with the aid of a hypodermic syringe, and the solution was transferred *via* a Teflon cannula to a 10 mm quartz fluorimeter cell equipped with a Teflon stopcock. The arene donor was added to the cell against a strong countercurrent of argon. The UV–VIS spectra of the [Ar, X–Py^+] complex was recorded before and after laser photolysis to ensure that only minimal diminution (< 10%) of the CT absorbance occurred during the transient spectroscopic experiment.

Time-resolved difference absorption spectra on the picosecond time-scale were obtained by utilizing either the 532 nm (second harmonic) or 355 nm (third harmonic) pulse from a Quantel YG 501-C mode-locked Nd^{3+}:YAG laser as the excitation source. The analysing light was generated by focussing the residual fundamental (1064 nm) on a mixture of H_2O and D_2O (1:1 v:v) contained in a 10 cm cuvette. The emergent white light was focussed on a bifurcated fibre-bundle (Dolan–Jenner) which directed the two analysing beams through the excited and unexcited volumes of the sample at a 90° angle to the excitation beam. The two analysing beams were collected by a fibre-optic cable and passed through a monochromator (ISA model HR-320) to a dual diode array (Princeton Instruments model DD-512) to record the signal. The monochromator was calibrated with the 436 nm and 542 nm lines from a mercury lamp. Time resolution was achieved by passing the fundamental (1064 nm) along a variable-delay stage (Velmex model B4036Q13). Before each spectral acquisition, a background data set was collected without exciting the sample. Absorbances were calculated using the relationship: $\Delta A = I_0 I^b / I_0{}^b I$, where I_0 represents the intensity of the analysing beam passing through the unexcited column of the sample and $I_0{}^b$ and I^b represent the intensities of the background. Spectra were acquired at a uniform excitation energy of 1.5 mJ per pulse, and they represented the average of 300 transients.

Time-resolved spectra on the nanosecond/microsecond timescale were obtained using the third harmonic (355 nm) of a Quantel YG 580-10 Q-switched Nd^{3+} : YAG laser with a 10 ns pulsewidth as the excitation source. The output of a 150 W Xenon arc lamp focussed on the sample at a 90° angle to the excitation beam served as the probe light. The probe beam emerging from the sample was focussed on the entrance slit of an Oriel model 77250 monochromator equipped with a model 77298 (500 nm blaze) grating in the spectral range between 300 and 800 nm. The monochromatic light was detected by a Hamamatsu model R-928 photomultiplier tube. The timing sequence of the excitation and probing of the sample was controlled by a Kinetics Instruments sequence generator and laser controller. Data acquisition and digitization were performed with a Tektronix model 7104 oscilloscope in conjunction with a Tektronix model C101 video camera and DCS-01 softward. The ns/μs spectral decays were processed with the ASYST (2.0) scientific software package.

Absorption Spectra and Extinction Coefficients of Aromatic Cation Radicals.—The aromatic cation radicals were generated by the triplet sensitization method of Das.[15] A solution of 0.01 mol dm^{-3} benzophenone, 0.10 mol dm^{-3} haloanisole and 0.05 mol dm^{-3} methylviologen (ditriflate salt) in degassed acetonitrile was irradiated at λ_{exc} = 355 nm using the Q-switched laser. Absorption bands due to the anisole radical ($BA^{+\bullet}$, λ_{max} = 500 nm; $CA^{+\bullet}$, λ_{max} = 460 nm) and the reduced methylviologen (λ_{max} = 390 and 610 nm) were observed and their absorbances decayed to baseline within 50 μs. Extinction coefficients were based on the equimolar formation of the haloanisole cation radical and the reduced methylviologen (ε at 610 nm = 14 000 dm^3 mol^{-1} cm^{-1}).[58] The absorbances of the anisole cations and $MV^{+\bullet}$ were compared on a time-scale (< 2 μs) at which there was negligible decay of the transients. Using the relationship: ε = 14 000 (A/A_{610}), where A is the $BA^{+\bullet}$ or $CA^{+\bullet}$ absorbance at λ_{max}, and A_{610} is the absorbance due to $MV^{+\bullet}$ at 610 nm, we obtained ε_{max} = 7800 and 8200 dm^3 mol^{-1} cm^{-1} for $CA^{+\bullet}$ or $BA^{+\bullet}$, respectively.

Computer Simulation of Picosecond Decays Using a Finite Laser Pulse-width.—A triangular (sawtooth) wave with zero intercepts at τ and $-\tau$ (τ = laser rise time) was used to simulate the spectral response of the kinetic system for which the quantum yield was taken as $\Phi = 1$. The analytical solution to the kinetics was separately calculated in three regions: Region I ($-\tau < t < 0$), Region II ($0 < t < \tau$) and Region III ($t > \tau$). The differential equations for the absorbance change of $ArH^{+\bullet}$ in eqn. (5) are given by: $dA/dt = (A_0/\tau)(1 + t/\tau) - k_1 A$ (Region I), $dA/dt = (A_0/\tau)(1 - t/\tau) - k_1 A$ (Region II) and $dA/dt = -k_1 A$ (Region III). Boundary conditions were applied by requiring the separate solutions for $A(t)$ to be equal at the boundaries of the three regions. The solution to this set of equations is given by: $A(t)/A_0 = (1/k_1\tau)(1 + t/\tau) - (1/k_1\tau)^2(1 - \exp[-k_1(t + \tau)])$ Region I; $A(t)/A_0 = (1/k_1\tau)(1 - t/\tau) - (1/k_1\tau)^2[1 - 2\exp(-k_1 t) + \exp[-k_1(t + \tau)]$ Region II; and $A(t)/A_0 = (1/k_1\tau)^2\exp[-k_1(t - \tau)] - 2\exp(-k_1 t) + \exp[-k_1(t + \tau)]$ Region III. Absorbances calculated for the various values of t/τ were used to generate the simulations in Fig. 6.

For the kinetics in Scheme 1, the contribution of the separate components T_1 and T_2 were calculated separately and added. The previously calculated solution, modified by replacing k_1

with $(k_1 + k_2) = \kappa$ gives the solution for T_1. Since $dT_2/dt = k_2[T_1](t)$, the solution for T_2 was obtained by integrating the expression for $T_1(t)$ term by term. This procedure gives the solution $T_2(t)/A_0 = (k_2/\kappa)(t/\tau + \frac{1}{2} + \tau^2/2\tau^2) - (k_2/\kappa)(1/\kappa\tau)$-$(1 + t/\tau) - (k_2/\kappa)(1/\kappa\tau)^2\{1 - \exp[-\kappa(t + \tau)]\}$ Region I; $T_2(t)/A_0 = k_2/\kappa(t/\tau + \frac{1}{2} - \tau^2/2\tau^2) - (k_2/\kappa)(1/\kappa\tau)$-$(1 - t/\tau) - (k_2/\tau)(1/\kappa\tau)^2\{1 - 2\exp(-\kappa\tau) + \exp[-\kappa(t + \tau)]\}$ Region II; and $T_2(t)/A_0 = k_2/\kappa - (k_2/\kappa)(1/\kappa\tau)^2\{\exp[-\kappa(t - \tau)] - 2\exp(-\kappa t) + \exp[-\kappa(t + \tau)]\}$ Region III. Since $T_1(t)$ tends to zero as t increases [the bracketed expression for $T_2(t)$ in Region II also tends to zero] it follows that for the lim $(t \rightarrow \infty)$, $T(t)/A_0 = k_2/\kappa = k_2/(k_1 + k_2)$. The solution for A_{max}, found by differentiating the solution to eqn. (5) is given by $A_{max} = (1/k_1\tau)\{1 - k_1\tau\ln [2 - \exp(-k_1\tau)]\} + (1/k_1\tau)^2\{1 - 2[2 - \exp(-\kappa t)^{-1}] + [2 - \exp(-\kappa\tau)^{-1}\exp(-\kappa\tau)\}$.

The rate constants k_1 and k_2 were obtained from the picosecond data as follows: for the [MA, $MePy^+$] complex in which $R = 0$, a graphical plot of A_{max}/A_0 as a function of k_1 was generated according to the expression $A_{max}/A_0 = (1/k_1\tau)\{1 - k_1\tau\ln[2 - \exp(-k_1\tau]\} + (1/k_1\tau)^2\{1 - 2[2 - \exp(-k_1\tau)]^{-1} + [2 - \exp(-k_1\tau)]^{-1}\exp(k_1\tau)\}$. Graphical interpolation on this curve using the value of A_{max}/A_0 obtained (0.05) yielded a value of $k_1 = 21\tau^{-1}$. The value of $\tau = 30$ ps (*vide infra*) yielded $k_1 = 7 \times 10^{11}$ s^{-1} for back electron transfer. For the bromoanisole-containing complexes, with R non-zero, the residual-dependent working curves were generated by differentiating T_1 and T_2 above, and setting the result to zero. This yielded the equation for $t_{max} = (1/\kappa\tau)\ \log(0.5\{1 + k\ (t_{max} - \tau) + \exp[-k(t_{max} + \tau)])$ where $\kappa = k_1 + k_2$. This expression was solved iteratively over an interval $0.1\tau^{-1} < \kappa < 5\tau^{-1}$ in which the iteration converged. The values of t_{max} so obtained were used to calculate the values of A_{max}/A_0 in Fig. 7 according to the expression above. Working curves generated using the experimental values of R in Table 2, and the values of κ were obtained from the experimental A_{max} by graphical interpolation as above. Since $A_{res}/A_o = k_2/(k_1 + k_2)$, the values of $k_1 + k_2$ could be calculated separately.

The value of τ, the laser pulse width, was obtained by photolysis of benzophenone in benzene. The transient absorbance at 530 nm (triplet–triplet—no decay on the 200 ps timescale of these measurements) was monitored and plotted as a function of time. The pulse time was calculated using the expression $\tau = t_{\frac{3}{4}} - t_{\frac{1}{4}}$ where $t_{\frac{3}{4}}$ and $t_{\frac{1}{4}}$ represent the times at which the absorbance reached $\frac{3}{4}$ and $\frac{1}{4}$ of its maximum (plateau) value. This procedure yielded a value of $= 30 \pm 3$ ps.

Charge-transfer Fluorination with N-Fluoropyridinium Salts.—All reactions were carried out under an inert argon atmosphere. Thermal reactions were shielded from roomlight. Photoreactions were carried out with a 500 W Hg lamp equipped with a suitable sharp cut-off filter (Corning Series CS-3) as follows.

Durene. A colourless solution of durene (60 μmol) and *N*-fluoropyridinium triflate (60 μmol) in acetonitrile (2 cm^3) was irradiated using a 300 nm cut-off filter. The solution became brown, and after 8 h, the solution was quenched with water and extracted with ether. GC analysis showed the presence of unchanged durene (15 μmol). GC–MS analysis indicated the presence of fluoro-2,3,5,6-tetramethylbenzene (0.8 μmol) [*m/z* 152 (46%), 151 (13), 138 (8.5), 137 (100), 133 (5.1), 115 (9.2), 109 (9.2)], 2,4,6-trimethylbenzyl fluoride (0.7 μmol) [*m/z* 152 (50%), 151 (13), 137 (100), 133 (5.8), 119 (74), 115 (19), 109 (9.6), 91 (18)] and 2,2′,3.4′,5,5′,6-heptamethyldiphenylmethane (4.3 μmol) [*m/z* 266 (35%), 251 (20), 146 (100), 132 (39), 147 (14), 133 (13), 131 (14), 117 (11), 115 (10), 91 (16)]. The fluorinated products were quantified with the calibration factor for durene. When 3,5-Cl_2PyF^+ was used as the acceptor, the pale yellow solution turned to brown upon irradiation using a 350 nm cut-off filter at 0 °C for 8 h. (The colourless solution of 3,5-dichloro-*N*-fluoropyridinium triflate in acetonitrile became yellow upon standing for a day without detectable loss of the cation, but not at 0 °C.) After aqueous work-up, the GC and GC–MS analyses of the ether extract indicated the presence of 2,4,5-trimethylbenzyl fluoride (1 μmol), 2,2′,3,4′,5,5′,6-heptamethyldiphenylmethane (17.5 μmol) and unchanged durene (20 μmol).

Pentamethylbenzene. The initially colourless solution from pentamethylbenzene (60 μmol) and *N*-fluoropyridinium triflate (60 μmol) in CH_3CN (2 cm^3) turned brown upon irradiation with a 300 nm cut-off filter at room temperature for 8 h. After aqueous work-up, GC and GC–MS analyses of the ether extract indicated the presence of pentamethylfluorobenzene (3 μmol) [*m/z* 166 (35%), 165 (8.3), 152 (11), 151 (100), 133 (5.4), 109 (7.7)], pentamethylbenzene dimer (9 μmol) [*m/z* 295 (14%), 294 (51), 279 (41), 161 (18), 160 (100), 147 (24), 146 (87), 145 (24)] and unchanged pentamethylbenzene (23 μmol). When a 3,5-Cl_2PyF^+ was used as the acceptor, the pale yellow solution turned brown after irradiation with a 350 nm cut-off filter at 0 °C for 5 h. The ether extract after aqueous work-up contained pentamethylfluorobenzene (1.2 μmol), tetramethylbenzyl fluoride (0.8 μmol) [*m/z* 166 (59%), 151 (100), 135 (28), 134 (13), 133 (85), 115 (18), 105 (12), 91 (23), 77 (15)], pentamethylbenzene dimer (5.7 μmol) and pentamethylbenzene (26 μmol) by GC and GC–MS analysis.

Hexamethylbenzene. The initially yellow solution from hexamethylbenzene (60 μmol) and 3,5-$Cl_2PyF^+OTf^-$ (60 μmol) turned brown after irradiation at >350 nm at 0 °C for 8 h. The ether extract after aqueous work-up contained *N*-pentamethylbenzylacetamide (2 μmol) [*m/z* 219 (19), 162 (21), 161 (17), 160 (100), 145 (35), 91 (10)] and hexamethylbenzene (43 μmol) by GC and GC–MS analysis.

1-*Methoxynaphthalene.* The yellow solution from 1-methoxynaphthalene (60 μmol) and 3,5-Cl_2PyF^+ (60 μmol) in CD_3CN (0.4 cm^3) was irradiated at >380 nm at 0 °C. After 4 h, 3,5-Cl_2PyF^+ was completely replaced by 3,5-Cl_2PyH^+ (52 μmol), as indicated by the ^1H NMR spectrum [δ_H 8.76 (d, 2 H), 8.64 (t, 1 H)]. In the ^{19}F NMR spectrum a resonance corresponding to 3,5-Cl_2PyF^+ disappeared and was replaced by three new resonances at δ_F 149.5, 150.1 and 153.0. After aqueous work-up, the ether extract contained three isomeric fluoro-1-methoxynaphthalenes (10, 8, 7 μmol). [Isomer 1: *m/z* 176 (54%), 162 (5.7), 161 (48), 134 (10), 133 (100), 107 (8.1), 83 (7.8), 63 (7.0); isomer 2 and 3 (overlapped) *m/z* 177 (7.2%), 176 (56), 162 (7.1), 161 (58), 134 (9.8), 133 (100), 107 (10), 83 (7.8), 63 (6.8), 57 (6.8)], trace (*ca.* 1 μmol) of difluoro-1-methoxynaphthalene [*m/z* 194 (56%), 180 (9.2), 179 (76), 163 (9.1), 152 (9.1), 151 (100), 75 (8.4)] and the aromatic dimer (6 μmol) [*m/z* 315 (23%), 314 (100), 300 (7.1), 299 (31), 268 (17), 267 (10), 255 (9.5), 239 (12.9), 226 (11.9), 113 (7.3)].

Naphthalene. The yellow solution of naphthalene (60 μmol) and 3,5-$Cl_2PyF^+OTf^-$ (51 μmol) in CD_3CN turned red-brown upon irradiation at >380 nm at 0 °C. After 3 h, 3,5-Cl_2PyF^+ nearly disappeared and 3,5-Cl_2PyH^+ (48 μmol) was formed when monitored by ^1H NMR analysis. The ^{19}F NMR analysis indicated the presence of 1-fluoronapthalene (19 μmol) at δ_F 126.5 (lit.,[59] 123.8), 2-fluoronaphthalene (1.5 μmol) at δ 117.7 (lit.,[59] 115.3) and HF (28 μmol) at δ 184.9.[25] The ether extract after aqueous work-up was analysed by HPLC (1-fluoronaphthalene and naphthalene were not resolved by gas chromatography). With an acetonitrile–water mixture (80:20 v:v) as the eluent, and *tert*-butylbenzene as the internal standard, naphthalene was quantified (25 μmol).

9-*Methylanthracene.* The red solution from 9-methylanthracene (60 μmol) and 3,5-$Cl_2PyF^+OTf^-$ (60 μmol) in CH_3CN (2 cm^3) slowly changed to a yellow orange solution, accompanied by a colourless precipitate. After 12 h, the solution was filtered and white solid (2.6 mg, 7 μmol) was identified as

lepidopterene[28] by ^{1}H NMR analysis. [$\delta_H(CDCl_3)$: 2.90 (d, 4 H, J = 2.7 Hz), 4.63 (t, 2 H, J = 2.7 Hz), 6.6–7.5 (m, 16 H).] The acetonitrile was evaporated and the residue was extracted with diethyl ether. NMR analysis of the ether layer indicated the presence of 9-fluoro-10-methylanthracene[27] (14 μmol) and 9-methylanthracene (5 μmol). 9-Fluoro-10-methylanthracene was separated from 9-methylanthracene by preparative silica gel TLC using pentane as the eluent. ^{1}H NMR of 9-fluoro-10-methylanthracene $\delta_H(CDCl_3)$ 3.05 (d, 3 H, J = 1.4 Hz), 7.53 (m, 4 H), 8.29 (m, 4 H); δ_F 136.9. The dichloromethane extract of the residue contained an unidentified product which showed no fluorine resonances. $\delta_H(CDCl_3)$ 3.19 (s), 7.1–8.3 (m). However, the solution of 9-methylanthracene (60 μmol) and 3,5-Cl_2PyF^+ (60 μmol) in CD_3CN (0.4 cm^3) was stable at 0 °C. After irradiation for 1 h at >480 nm at 0 °C, the solution consisted of 9-fluoro-10-methylanthracene (13 μmol), lepidopterene (10 μmol), unidentified product, 9-methylanthracene (5.7 μmol), and 3,5-Cl_2PyH^+ (55 μmol) by ^{1}H NMR analysis and HF (41 μmol) by ^{19}F NMR analysis. Control experiments carried out in the dark showed no detectable change within the same time period.

Electrophilic and Charge-transfer Fluorination of Dimethoxynaphthalene.—The thermal reaction of 2,6-dimethoxynaphthalene (60 μmol) and 3,5-dichloro-*N*-fluoropyridinium triflate (60 μmol) was carried out in CD_3CN (0.4 cm^3) at room temperature in the dark. The initially red-orange colour slowly bleached, and after 2 days the ^{1}H NMR resonances corresponding to the 3,5-dichloro-*N*-fluoropyridinium moiety were completely replaced by those of *N*-protonated 3,5-dichloropyridine (52 μmol). In the ^{19}F NMR spectrum, the resonance corresponding to that of 3,5-dichloro-*N*-fluoropyridinium disappeared and was replaced by a single resonance at 136.6 ppm, which accounted 55 μmol of a single fluorine compound (by integration relative to the triflate resonance). After evaporation of the solvent, the ether extract contained a single fluoro-2,6-dimethoxynaphthalene by GC and GC–MS analysis. [*m*/*z* 206 (74%), 192 (13), 191 (100), 163 (87), 148 (34), 132 (17), 131 (9.8), 120 (56)]. A pure sample was obtained by silica gel chromatography using a mixture of ethyl acetate and light petroleum (5:95, v:v) as the eluent (R_f = 0.20). $\delta_H(CDCl_3)$ 3.90 (s, 3 H), 3.99 (s, 3 H), 7.1–7.5 (m, 4 H), 7.94 (d, 1 H, J = 8.8 Hz) [Found: C, 69.65; H, 5.4. Calc. for $C_{12}H_{11}FO_2$ (*M*, 206.2): C, 69.88; H, 5.39%]. The corresponding photoreaction was carried out with 2,6-dimethoxynaphthalene (60 μmol) and 3,5-$Cl_2PyF^+OTf^-$ (60 μmol) in acetonitrile (2 cm^3) using the 415 nm cut-off filter at 0 °C. After 3 h of irradiation, the reaction mixture was quenched with water, and the ether extract was found to contain the fluoro-2,6-dimethoxynaphthalene (29 μmol) which was identical with that obtained in the thermal reaction (GC, GC–MS and ^{1}H NMR analyses). Other components in the ether fraction were unchanged 2,6-dimethoxynaphthalene (12 μmol) and difluoro-2,6-dimethoxynaphthalene (*ca.* 2 μmol) by GC and GC–MS [*m*/*z* 224 (85%), 210 (12), 209 (100), 181 (84), 166 (43), 150 (18), 138 (47)].

Charge-transfer Acetoxylation and Methylation of Aromatic Donors with N-*Acetoxypyridinium Salts.*—*N*-Acetoxy-4-cyanopyridinium salts do not react thermally with aromatic donors when monitored spectrally (^{1}H NMR) or by the quantitative recovery of the aromatic donor. The charge-transfer photoreactions were carried out with a solution of 60 μmol 4-$NCPyOAc^+$ and 60 μmol aromatic donor in 2 cm^3 of acetonitrile (using a suitable cut-off filter).

Anthracene. Acetoxyanthracene (M^+, 236) and 9-methylanthracene were identified by GC and GC–MS analysis.

Pentamethylbenzene. Afforded pentamethylphenyl acetate (2 μmol) [*m*/*z* 206 (17%), 165 (13), 164 (100), 150 (13), 149 (93), 105 (16), 91 (17)], hexamethylbenzene (1 μmol), and nonamethyldiphenylmethane (1 μmol).

2,6-*Dimethoxynaphthalene* yielded acetoxy-2,6-dimethoxynaphthalene (3 μmol) [*m*/*z* 246 (20%), 205 (9.7), 204 (82), 190 (11), 189 (100), 161 (29), 160 (10)], and methyl-2,6-dimethoxynaphthalene (0.5 μmol) [*m*/*z* 203 (15%), 202 (100), 188 (14), 187 (88), 159 (47), 144 (29), 129 (9.6), 128 (20), 127 (16), 116 (17), 115 (31)]. The photoreactions of durene and naphthalene were monitored by ^{1}H NMR spectroscopy. In both cases, 4-$NCPyOAc^+$ was decomposed but other than the appearance of 4-$NCPyH^+$ the aromatic donor was essentially unchanged. In the photoreaction of 9-methylanthracene, after 15 h 60% of the 4-$NCPyOMe^+$ disappeared, and 80% unchanged 9-methylanthracene was found in addition to *ca.* 10% of lepidopterene.

Charge-transfer Methoxylation of Aromatic Donors with N-*Methoxypyridinium Salts.*—*N*-Methoxypyridinium salts did not react thermally with aromatic donors at room temperature in the dark. However, upon irradiation, the reaction mixture became brown and was worked up in the usual manner.

Anthracene afforded methoxyanthracene as the sole product (M^+, 208).

2,6-*Dimethoxynaphthalene* gave methoxy-2,6-dimethoxynaphthalene(s) as product(s) (M^+, 218).

9-*Methylanthracene.* The red solution from 9-methylanthracene (60 μmol) and 4-$NCPyOMe^+$ (60 μmol) in CD_3CN (0.4 cm^3) was irradiated using a 460 nm cut-off filter and the progress of reaction was monitored by ^{1}H NMR spectroscopy. After 40 h, 10 μmol of 4-$NCPyOMe^+$ remained and 45 μmol of 4-$NCPyH^+$ appeared. NMR analysis also indicated the presence of 9-methoxy-10-methylanthracene[29] (25 μmol), unchanged 9-methylanthracene (17 μmol), traces of lepidopterene (1 μmol) and other unidentified products.

Hexamethylbenzene yielded methyl pentamethylbenzyl ether (*ca.* 0.5 μmol), [*m*/*z* 192 (21%), 176 (14), 175 (18), 161 (41), 160 (100), 147 (25), 145 (41), 133 (13), 105 (12), 91 (15)] and bibenzylic dimers (0.5 μmol) [*m*/*z* 323 (7.8%), 322 (31), 162 (11), 161 (100)].

Naphthalene. After 12 h, approximately 70% of the 4-$NCPyOMe^+$ disappeared to give unidentified product(s), but 70% of the naphthalene was recovered.

Acknowledgements

We thank the National Science Foundation, the Robert A. Welch Foundation and the Texas Advanced Research Project for financial support.

References

1 G. A. Olah, R. Malhotra and S. C. Narang, *Nitration*, VCH, New York, 1989.
2 T. Umemoto, S. Fukami, G. Tomizawa, K. Harasawa, K. Kawada and K. Tomita, *J. Am. Chem. Soc.*, 1990, **112**, 8563.
3 Z. Q. Shi, unpublished results.
4 S. Sankararaman and J. K. Kochi, *J. Chem. Soc., Perkin Trans. 2*, 1991, 1.
5 E. K. Kim, K. Y. Lee and J. K. Kochi, *J. Am. Chem. Soc.*, 1992, **114**, 1756.
6 K. Y. Lee and J. K. Kochi, *J. Chem. Soc., Perkin Trans. 2*, 1992, 1011.
7 R. S. Mulliken, *J. Am. Chem. Soc.*, 1950, **72**, 601; 1952, **74**, 811.
8 R. S. Mulliken and W. B. Person, *Molecular Complexes*, Wiley, New York, 1969.
9 J. K. Kochi, *Acta Chem. Scand.*, 1990, **44**, 409.
10 See: J. H. Ridd, *Chem. Soc. Rev.*, 1991, **20**, 149.
11 H. Tsubomura and R. S. Mulliken, *J. Am. Chem. Soc.*, 1960, **82**, 5966. See also T. M. Bockman, H. R. Chang, H. G. Drickamer and J. K. Kochi, *J. Phys. Chem.*, 1990, **94**, 8483.

12 R. Foster, *Organic Charge-Transfer Complexes*, Academic Press, New York, 1969.
13 H. Masuhara, H. Miyasaka, T. Karen, T. Uemiya, N. Mataga, M. Koishi, A. Takeshima and Y. Tsuchiya, *Opt. Commun.*, 1984, **44**, 426.
14 S. Sankararaman, W. A. Haney and J. K. Kochi, *J. Am. Chem. Soc.*, 1987, **109**, 7824.
15 P. K. Das, *J. Chem. Soc., Faraday Trans. 1*, 1983, **79**, 1135.
16 K. Sehested, J. Holcman and E. J. Hart, *J. Phys. Chem.*, 1977, **81**, 1363.
17 T. Yabe, S. Sankararaman and J. K. Kochi, *J. Phys. Chem.*, 1991, **95**, 4177.
18 M. Itoh and S. Nagakura, *J. Am. Chem. Soc.*, 1967, **89**, 3959.
19 (*a*) R. R. Alfano and S. L. Shapiro, *Phys. Rev. Lett.*, 1970, **24**, 584; (*b*) S. M. Hubig and M. A. J. Rodgers, in *Handbook of Organic Photochemistry*, vol. 1, ed. J. C. Scaiano, CRC Press, Boca Raton, Florida, 1989, p. 319 ff.
20 S. Sankararaman and J. K. Kochi, *J. Chem. Soc., Perkin Trans. 2*, 1991, 165.
21 *cf.* S. Sankararaman, S. Perrier and J. K. Kochi, *J. Am. Chem. Soc.*, 1989, **111**, 6448.
22 (*a*) R. O. C. Norman, C. B. Thomas and J. S. Willson, *J. Chem. Soc., Perkin Trans. 1*, 1973, 326; (*b*) W. Lau and J. K. Kochi, *J. Am. Chem. Soc.*, 1984, **106**, 7100.
23 A. Bewick, G. J. Edwards, J. M. Mellor and S. Pons, *J. Chem. Soc., Perkin Trans. 2*, 1977, 1952.
24 E. K. Kim, T. M. Bockman and J. K. Kochi, to be submitted for publication.
25 K. O. Christe and W. W. Wilson, *J. Fluorine Chem.*, 1990, **46**, 339.
26 F. Radner, *J. Org. Chem.*, 1988, **53**, 704.
27 P. F. King and R. F. O'Malley, *J. Org. Chem.*, 1984, **49**, 2803.
28 L. A. Deardurff, M. S. Alnajja and D. M. Camaioni, *J. Org. Chem.*, 1986, **51**, 3686.
29 A. D. Mosnaim, D. C. Nonhebel and J. A. Russell, *Tetrahedron*, 1970, **26**, 1123.
30 P. L. Majumder and M. Joardar, *Indian J. Chem.*, 1983, **22B**, 1191.
31 Y. Hirata, Y. Kanda and N. Mataga, *J. Phys. Chem.*, 1983, **87**, 1659.
32 I. R. Gould, R. H. Young, R. E. Moody and S. Farid, *J. Phys. Chem.*, 1991, **95**, 2068.
33 Y. Takahashi, S. Sankararaman and J. K. Kochi, *J. Am. Chem. Soc.*, 1989, **111**, 2954.
34 (*a*) E. M. Kosower, *Top. Curr. Chem.*, 1983, **112**, 117; (*b*) E. M. Kosower and E. J. Poziomek, *J. Am. Chem. Soc.*, 1964, **86**, 5515.
35 T. Muramatsu, Y. Ikegami, K. Hanaya and S. Onodera, *Bull. Chem. Soc. Jpn.*, 1990, **63**, 1413.
36 I. Carelli, *Electrochim. Acta*, 1990, **35**, 1185.
37 T. M. Bockman and J. K. Kochi, *J. Am. Chem. Soc.*, 1989, **111**, 4699.
38 E. T. Kaiser and L. Kevan, *Radical Ions*, Wiley, New York, 1968.
39 I. Carelli, M. E. Cardinali, A. Casini and A. Arnone, *J. Org. Chem.*, 1976, **41**, 3967.
40 S. Ehrenson, R. T. C. Brownlee and R. W. Taft, *Prog. Phys. Org. Chem.*, 1973, **10**, 1.
41 R. A. Marcus, *J. Chem. Phys.*, 1956, **24**, 966. See also: R. A. Marcus, *Ann. Rev. Phys. Chem.*, 1964, **15**, 155 and L. Eberson, *Electron Transfer Reactions in Organic Chemistry*, Springer, New York, 1987.
42 *cf.* K. Y. Lee, C. Amatore and J. K. Kochi, *J. Phys. Chem.*, 1991, **95**, 1285.
43 H. Lemmetyinen, J. Konijnenberg, J. Cornelisse and C. A. G. O. Varma, *J. Photochem.*, 1985, **30**, 315.
44 P. S. Skell, H. N. Baxter, III, J. M. Tanko and V. Chebolu, *J. Am. Chem. Soc.*, 1986, **108**, 6300.
45 M. J. Perkins in *Free Radicals*, vol. 2, ed. J. K. Kochi, Wiley, New York, 1973, p. 231 ff.
46 H. C. Christensen, K. Sehested and E. J. Hart, *J. Phys. Chem.*, 1973, **77**, 983.
47 F. A. Cotton and G. Wilkinson, *Advanced Inorganic Chemistry*, 5th edn., Wiley, New York, 1988, p. 324.
48 (*a*) M. L. Poutsma in *Free Radicals*, vol. 2, ed. J. K. Kochi, Wiley, New York, 1973, p. 159 ff; (*b*) J. K. Kochi, *Free Radicals*, p. 665 ff.
49 K. U. Ingold in *Free Radicals*, vol. 1, ed. J. K. Kochi, Wiley, New York, 1973, p. 37 ff.
50 See: K. Yoshida, *Electro-oxidation in Organic Chemistry*, Wiley, New York, 1984.
51 (*a*) C. J. Schlesener, C. Amatore and J. K. Kochi, *J. Am. Chem. Soc.*, 1984, **106**, 3567; (*b*) J. M. Masnovi, S. Sankararaman and J. K. Kochi, *J. Am. Chem. Soc.*, 1989, **111**, 2263.
52 (*a*) I. P. Beletskaya and D. I. Makhon'kiv, *Russ. Chem. Rev.*, 1981, **50**, 534; (*b*) O. Hammerich and V. D. Parker, *Adv. Phys. Org. Chem.*, 1984, **20**, 55; (*c*) L. Eberson and K. Nyberg, *Acc. Chem. Res.*, 1973, **6**, 106; (*d*) W. Lau and J. K. Kochi, *J. Am. Chem. Soc.*, 1986, **108**, 6720.
53 K. L. Rollick and J. K. Kochi, *J. Am. Chem. Soc.*, 1982, **104**, 1319.
54 E. Baciocchi, *Acta Chem. Scand.*, 1990, **44**, 645.
55 A. McKillop, A. G. Turrell, D. W. Young and E. C. Taylor, *J. Am. Chem. Soc.*, 1980, **102**, 6504.
56 W. Braun, L. Rajbenbach and F. R. Eirich, *J. Phys. Chem.*, 1962, **66**, 1591.
57 J. K. Kochi, *Angew. Chem., Int. Ed. Engl.*, 1988, **27**, 1227. See also ref. 9.
58 T. Watanabe and K. Honda, *J. Phys. Chem.*, 1982, **86**, 2617.
59 S. Singh, D. D. DesMarteau, S. S. Zuberi, M. Witz and H.-N. Huang, *J. Am. Chem. Soc.*, 1987, **109**, 7194.

Paper 2/01806C
Received 6*th April* 1992
Accepted 14*th May* 1992